BBA - Molecular Basis of Disease 1865 (2019) 1152–1159

Contents lists available at ScienceDirect

BBA - Molecular Basis of Disease

journal homepage: www.elsevier.com/locate/bbadis

The nitrone spin trap 5,5-dimethyl-1-pyrroline *N*-oxide binds to *toll*-like receptor-2-TIR-BB-loop domain and dampens downstream inflammatory signaling

Marcos D. Muñoz[a], Lucas J. Gutierrez[b], Sandrine Delignat[c,d,e], Jules Russick[c,d,e], Sandra E. Gomez Mejiba[f,*], Sebastien Lacroix-Desmazes[c,d,e], Ricardo D. Enriz[b,*], Dario C. Ramirez[a,*]

[a] Laboratory of Experimental and Translational Medicine, IMIBIO-SL-School of Chemistry, Biochemistry and Pharmacy, National University of San Luis-CONICET, San Luis, 5700 San Luis, Argentina
[b] Laboratory of Medicinal Chemistry, IMIBIO-SL-School of Chemistry, Biochemistry and Pharmacy, National University of San Luis-CONICET, San Luis, 5700 San Luis, Argentina
[c] INSERM, UMR S 1138, Centre de Recherche des Cordeliers, F-75006 Paris, France
[d] Université Pierre et Marie Curie-Paris6, UMR S 1138, Centre de Recherche des Cordeliers, F-75006 Paris, France
[e] Université Paris Descartes, UMR S 1138, Centre de Recherche des Cordeliers, F-75006 Paris, France
[f] Laboratory of Experimental Therapeutics, IMIBIO-SL, School of Health Sciences, National University of San Luis-CONICET, San Luis, 5700 San Luis, Argentina

ARTICLE INFO

Keywords:
TLR2
DMPO
Signal transduction
TIR domain
BB-loop
Mechanism-based drug

ABSTRACT

The nitrone spin trap 5,5-dimethyl-1-pyrroline *N*-oxide (DMPO) dampens endotoxin-induced and TLR4-driven priming of macrophages, but the mechanism remains unknown. The available information suggests a direct binding of DMPO to the TIR domain, which is shared between TLRs. However, TLR2-TIR domain is the only TLR that have been crystallized. Our *in silico* data show that DMPO binds to four specific residues in the BB-loop within the TLR2-TIR domain. Our functional analysis using hTLR2.6-expressing HEKs cells showed that DMPO can block zymosan-triggered-TLR2-mediated NF-κB activation. However, DMPO did not affect the overall TLR2-MyD88 protein-protein interaction. DMPO binds to the BB-loop in the TIR-domain and dampens downstream signaling without affecting the overall TIR-MyD88 interaction. These data encourage the use of DMPO-derivatives as potential mechanism-based inhibitors of TLR-triggered inflammation.

1. Introduction

Spin traps are low-molecular-weight compounds that covalently bind to radical sites in radicalized molecules, and thus can stop free radical chain reactions that otherwise end in end-oxidation products [1]. Nitrone spin traps such as *N-tert*-butyl-α-phenylnitrone (PBN) and 5,5-dimethyl-1-pyrroline *N*-oxide (DMPO) were originally developed with the purpose of trapping and stabilizing free radicals, thus making possible their study by electron spin resonance or immuno-spin trapping [2,3]. However, these nitrones have been proved to have anti-inflammatory properties on several experimental models [4]. Both spin traps are able to dampen lipopolysaccharide (LPS)-triggered signaling related to mitogen-activated protein kinase, protein kinase B, inducible nitric oxide synthase, cyclooxygenase-2 and pro-inflammatory cytokines [5,6] suggesting that these effects may be related to their nitrone motif. These anti-inflammatory effects are unlikely to be related to their free radical trapping properties because of the low reaction rate constant of this reaction [7].

Currently, DMPO or any of its structural analogs, have not been moved into the drug development pipeline. That may be due to DMPO synthesis being really expensive in comparison to PBN and its derivatives. PBN-analogs have been synthesized and their anti-inflammatory properties have been tested in different experimental models [4,8]. Moreover, some of them have reached phase III clinical trials, but the

Abbreviations: DMPO, 5,5-dimethyl-1-pyrroline *N*-oxide; MD, molecular dynamics; IPA, Ingenuity Pathway Analysis; LPS, lipopolysaccharide; QTAIM, Quantum Theory of Atoms In Molecules; TLR2, *toll*-like receptor 2; TIR, *toll*-interleukin-1 receptor; NF-κB, nuclear factor kappa-light-chain-enhancer of activated B cells; PBN, *N-tert*-butyl-α-phenylnitrone; MyD88, myeloid differentiation primary response 88; SEAP, secreted alkaline phosphatase; PMA, phorbol 12-myristate 13-acetate; BCPs, bond critical points

* Corresponding authors at: IMIBIO-SL-UNSL-CONICET, Chacabuco 917, Fist floor, Box 13X, San Luis, 5700 San Luis, Argentina.
E-mail addresses: segomez@unsl.edu.ar (S.E. Gomez Mejiba), denriz@unsl.edu.ar (R.D. Enriz), dramirez@unsl.edu.ar (D.C. Ramirez).

https://doi.org/10.1016/j.bbadis.2019.01.005
Received 21 October 2018; Received in revised form 23 December 2018; Accepted 2 January 2019
Available online 23 January 2019
0925-4439/

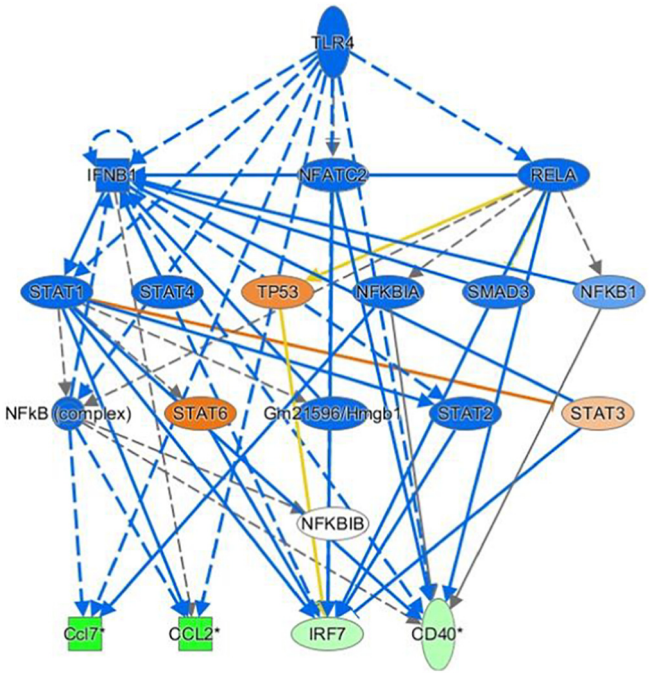

Fig. 1. TLR4 predicted as inhibition by IPA software analysis on the transcriptome of LPS-primed RAW 264.7 cells in the presence of DMPO. Figure displays how molecules predicted (blue) are related to each other and the behavior of genes downstream of these interactions. Solid lines correspond to direct physical interactions. Dashed lines correspond to indirect interactions. CCL2, CCL7, IRF7, and CD40 are highlighted in green indicating down-regulation of its mRNAs expression in the DMPO + LPS *vs* LPS comparison. It is important to highlight that most of the upstream regulators are predicted as inhibitions, which is consistent with DMPO dampening the entire signaling related to LPS-triggered TLRs signaling. Extracted from *Muñoz et al.* [11].

mechanisms behind these effects remain obscure [4].

By using DMPO as a tool we have studied the intracellular localization and identity of radicalized protein in cells, tissues and whole animals [9,10]. Interestingly, DMPO dampened LPS-driven RAW264.7-macrophage-like cell line activation, thus prevented nitric oxide and inflammatory chemokine production. These effects afforded by DMPO were linked to inhibition of nuclear factor kappa-light-chain-enhancer of activated B cells (NF-κB) signaling pathway at early time points after the stimulus (*i.e.,* 15 min) [5]. We have also studied the effects of DMPO on the transcriptome of macrophages and found that the spin trap was able to change the expression of 215 genes when added simultaneously with LPS on RAW 264.7 cells for 6 h. Interestingly, 75% of those genes were downregulated when compared to LPS stimulated cells. Functional analysis of these genes using Ingenuity Pathway Analysis (IPA) software was consistent with a negative regulation of the innate immune system with several *toll*-like receptors (TLR-4, -3 and -9) indicated as receptors being affected by DMPO [11] (Fig. 1). Currently, the exact mechanism by which spin traps exert their anti-inflammatory effects remains unknown. However, the production of mechanism-based drugs is an emerging field that will lead to safer anti-inflammatory drugs. This can be moved forward by knowing the exact changes in transcriptome, proteome, and phenome induced by DMPO in inflammatory cells, such as macrophages. In this regard, transcriptomic and functional changes induced by DMPO in macrophages, as we have recently reported [11], may be an important step towards accomplishing this goal.

Toll-like receptors sense conserved pathogen- and danger-associated molecular patterns released by microbes and the host [12]. Among the most studied TLRs, TLR4 is well known because of its participation in inflammatory response triggered by LPS. Closely related, TLR2 binds peptidoglycan and it is necessary for the correct signaling triggered by LPS throughout TLR4 [13,14]. Interestingly, all TLRs have in common a cytoplasmic domain called toll-interleukin-1 receptor (TIR) that mediates interactions with adaptor molecules such as myeloid differentiation primary response 88 (MyD88) and *Toll*-interleukin 1 receptor domain containing adaptor protein (TIRAP) [15]. A region called BB-loop within the TIR domain has been pointed as a critical region for a successful TLR downstream signal transduction. Indeed, a site-directed mutation of one residue at the BB-loop (called after the β-sheet and α-helix motifs that compose the tridimensional structure) region (P712 in murine TLR4 and its analog on human TLR2-P681) results in signal impairment [16,17]. This evidence points the BB-loop within the TLR's TIR domain as a rational target for attenuation of TLRs signaling. To the date, TLR4-TIR domain has not yet been crystallized making impossible to perform *in silico* studies on this receptor's domain. On the other hand, TLR2-TIR domain has already been crystallized and has many structural and functional similarities with TLR4 [13,14] making it a suitable experimental model for docking and molecular dynamics studies on TLR-TIR signaling.

These pieces of evidence led us to hypothesize that the anti-inflammatory effects of DMPO can be explained by direct binding of the spin trap to the TIR domain of TLRs. To test this hypothesis we combined *in silico* techniques of docking, molecular dynamics simulations and QTAIM (Quantum Theory of Atoms In Molecules) calculations to determine the site and strength of the interaction between DMPO and TLR2 TIR domain, as well as biochemical techniques to determine the functional significance of our findings.

2. Materials and methods

2.1. Blind docking setup

The three-dimensional crystal structure of TLR2 TIR domain employed in this work was obtained from the Protein Data Bank ID code 1FYW. This structure was subjected to energy minimization calculations to remove possible bumps using the Amber16 package.

The docking simulations were carried out using of AutoDock 4.2 [18]. The docking of the DMPO was performed on the entire TLR2 TIR domain surface without prior specification of the binding site ("blind docking"). In docking experiments the following parameters were used: the initial population of trial ligands was composed of 250 individuals; the maximum number of generations was set to 270,000. The maximum number of energy evaluations was 10.0×10^6. All other parameters were maintained at their default setting. The 3D affinity map was a cube with $126 \times 126 \times 126$ points separated by 0.375 Å and centered at the TLR2-TIR domain. The resulting docked conformations were clustered into families by the backbone rmsd. The lowest docking-energy conformation for each family was considered as the most favorable orientation.

2.2. Refinement of the anchoring/binding mode

After the docking calculations, leading lowest energy structures were refined by performing molecular dynamics simulations, using the Amber16 packet. The molecular dynamics simulations (MD) were performed using the all-atom force field ff99SB [19] to describe the receptor, whereas the general Amber force field (GAFF) [20] was used to handle small organic molecules and the force field parameters of the inhibitors were produced by the antechamber program in Amber. The water molecules were represented by the TIP3P model. Each model was soaked in a truncated octahedral-periodic box of TIP3P water molecules. The distance between the edges of the water box and the closest atom of the solutes was at least 10 Å. Sodium ions were added to neutralize the charge of the system. The entire system was subjected to energy minimization.

Next, each system was heated in the NVT ensemble from 100 to 300 K in 500 ps and equilibrated at an isothermal-isobaric (NPT)

ensemble for another 500 ps. A Langevin thermostat [21] was used for temperature coupling with a collision frequency of 1.0 ps^{-1}. The Particle Mesh Ewald (PME) method was employed to treat the long-range electrostatic interactions in a periodic boundary condition [22]. The SHAKE method was used to constrain hydrogen atoms. The time step for all MD is 2 fs, with a direct-space, non-bonded cut-off of 8 Å. Finally, the production was performed at the NPT ensemble by running three independent simulations with length limited to 20 ns, accounting for a total simulation length of 60 ns. The only difference between replicates was the initial velocity assignments at the beginning of the dynamics.

2.3. The MM-PBSA method

In MM-PBSA [23], the binding free energy (ΔGbind) resulting from the formation of an RL complex between a ligand (L) and a receptor (R) is calculated as:

DGbind = Gcomplex − (Gprotein + Ginhibitor)

G = Egas + Gsolve − TS

Egas = Einternal + Eelectrostatic + Evdw

Gsolve = GPB + GSASA

where ΔEMM, ΔGsol, and -TΔS are the changes of the gas phase MM energy, the solvation free energy, and the conformational entropy upon binding, respectively. ΔEMM includes ΔEinternal (bond, angle, and dihedral energies), ΔEelectrostatic (electrostatic), and ΔEvdw (van der Waals) energies. ΔGsolv is the sum of electrostatic solvation energy (polar contribution), ΔGGB, and the non-electrostatic solvation component (nonpolar contribution), ΔGSA. The polar contribution is calculated using the GB model, while the nonpolar energy is estimated by solvent accessible surface area (SASA). The conformational entropy change, -TΔS, is usually computed by normal-mode analysis, but in this study, the entropy contributions were not calculated due to the computational cost involved in such calculations.

2.4. QM/MM setup

A two-layer ONIOM (QM/MM) method has been used [24]. The compound DMPO and the side chains of the residues that have at least one heavy atom within 5 Å from the ligand molecule was incorporated into the high-level QM layer and the remainder of the complex system was included in the low-level MM layer. The QM region was calculated using the M062X/6-31G(d) method [25] and the MM portion using the AMBER force field [20,26]. The MM parameters absent in the standard AMBER force field were included from the generalized AMBER force field [20]. Only the geometry of the QM layer was fully optimized.

2.5. Atoms in molecules theory

From the Quantum Theory Atoms In Molecules (QTAIM) point of view, two interacting atoms share three topological elements related to each other, a point, a line, and a surface. The first element is the bond critical point (BCP), namely the critical point in ρ(r) topology that is found between any two interacting nuclei. From each BCP, two unique trajectories of gradient vectors of electronic density, ∇ρ(r), originate at that point and terminate at each of the neighboring nuclei. These trajectories define a line along in which ρ(r) is a maximum with respect to any neighboring line. This line that constitutes the second element is the bond path (BP). Additionally, the set of trajectories that terminate at a BCP define the interatomic surface that separates the atomic basins of the neighboring atoms. The topological properties of a scalar field such as ρ(r) are summarized in terms of their critical points (*i.e.*, the points rc where Δρ(r) = 0). Critical points are classified according to their type (ω, σ) by stating their rank (ω), and signature (σ). Critical points of (3, −1) and (3, +1) type describe saddle points, while the (3, −3) is a maximum and (3, +3) is a minimum in the field. Among these critical points, the (3, −1) or bond critical point was used to describe ligand-receptor interactions. The wave functions of the inhibitor complexed to the binding site residues (residues that have at least one heavy atom within 5 Å from the DMPO molecule) were generated at the M062X/6-31G(d) level of theory. Such systems were subjected to a QTAIM analysis [27] using Multiwfn software [28]. This type of calculations has been used in recent works because it ensures a reasonable compromise between the wave function of enough quality to obtain reliable values of the derivatives of ρ(r) and the computer power available, due to the extension of the analyzed systems [29–31].

2.6. Gene-reporter assay for NF-κB activity in hTLR2.6 expressing HEK293 cells

HEK293 cells transfected with human TLR2.6 (hTLR2.6) were obtained from Invivogen and grown in DMEM (GIBCO, Cat#11995073) supplemented with 10% fetal calf serum (FCS, Biowest, Cat# S1810) and 10 μg/mL blasticidin S (Invivogen Cat#A1113903). The day of the experiment cells (3.10^4 cells/100 μL) were seeded in 96-well plates for 24 h before transfection. The cells were transiently transfected with the NF-κB-driven secreted alkaline phosphatase (SEAP) reporter construct (pNiFty-SEAP, Invivogen, Cat# 17C17-MM) using Lipofectamine 2000™ (Invitrogen, Cat#11668–019). After a 24 h-exposure to the transfection mixture, the cells were stimulated for 24 h with 66.7 μg/mL zymosan (Sigma, Cat#58856-93-2) and/or 50 mM DMPO (Dojindo, Cat#D048-10). SEAP activity in the cell supernatants was measured by a colorimetric assay using the QUANTI-Blue™ substrate (Invivogen, Cat#18A22-MM). QUANTI-Blue™ medium changes to a purple-blue color in the presence of SEAP. Optical densities were measured by a microplate reader (GENios, TECAN) at 620 nm. All experiments were independently repeated at least 3 times with triplicates within each plate.

2.7. MyD88-TLR2 co-immunoprecipitation

THP-1 cells (American Type Culture Collection, Cat#TIB-202™) were cultured in RPMI 1640 medium (Gibco, Cat#R0883) modified to contain 2 mM L-glutamine, 4500 mg/L glucose, and 1500 mg/L sodium bicarbonate, and were supplemented with 10% (vol/vol) heat-inactivated FCS. THP-1 cells were plated at 5×10^6 cells per well in T-25 ml tissue bottles with 50 ng/mL phorbol 12-myristate 13-acetate (PMA, Sigma, Cat#P1585-1MG) for 24 h. Adherent cells were rinsed with phosphate-buffered saline (PBS) and then treated with 100 μg/mL zymosan (Sigma, Cat#58856-93-2) in the presence or in the absence of 50 mM DMPO for 15 min. After incubation, cells were rinsed with ice-cold PBS and whole-cell proteins were extracted using Mild Lysis Buffer containing 50 mM TRIS (pH 7.4), 150 mM NaCl, 20 mM NaF, 1% Igepal, 1 mM Na_3VO_4 and protease inhibitor (Roche Applied Science, Cat#11 836 153 001). Proteins extracted were quantified using BCA Protein Assay Reagents (Thermo Scientific/Pierce, Cat#23225) and incubated with the anti-TLR2 antibody (Santa Cruz Technologies, Cat#sc-21760) overnight at 4 °C with rotation. Prewashed 50 uL protein G-agarose (Roche, Cat#11 243 233 00) was added to each sample and rotated at 4 °C for 4 h. Beads were then washed three times in lysis buffer (without protease inhibitor) and finally in complete lysis buffer. Beads were re-suspended in 4× Laemmli sample buffer and boiled for 10 min. Immunoprecipitated proteins were separated by 4–12% SDS/PAGE, transferred onto a nitrocellulose membrane, blocked, and incubated with the anti-TLR2 antibody, and anti-Myd88 antibody (Santa Cruz Technologies, Cat#sc-11356) for 1 h. Development was carried out using HRP-linked secondary antibody (Santa Cruz Technologies, Cat#sc-516102) and bands were visualized using ECL Plus Reagents (Amersham Pharmacia Biotech, Cat#RPN2132) in a myECL imager (ThermoScientific/Pierce). Band intensity was analyzed using ImageJ software [32]. Results are shown as TLR2-My88 ratio of 3 independent

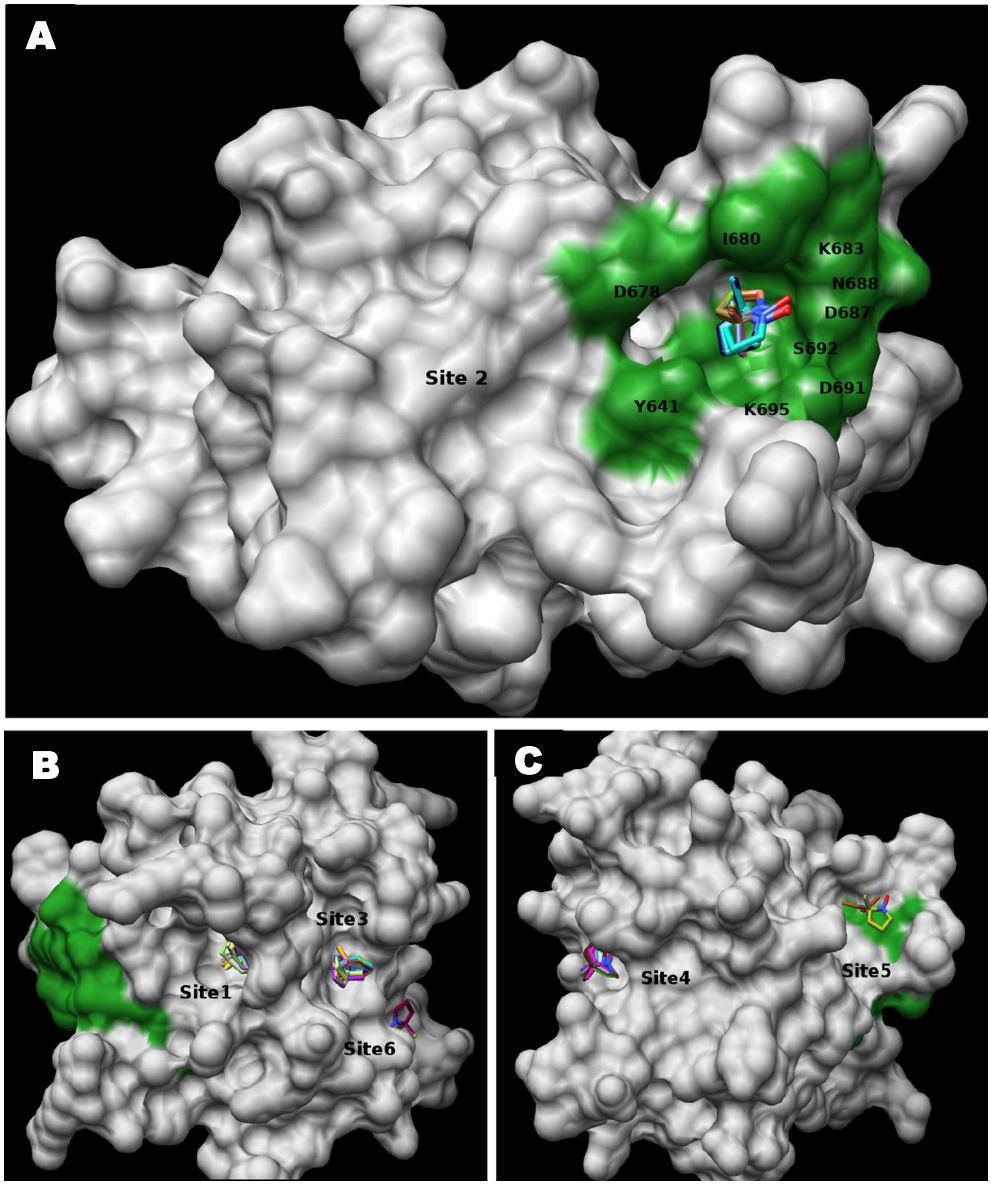

Fig. 2. Topographic location of the six DMPO-binding sites at the TLR2-TIR domain as found from the blind docking procedure. The TIR domain is shown in white color; whereas the spatial location of the preferred six DMPO-binding sites is shown in green. A) Site 2 and residues involved in DMPO binding. B) Sites 1, 3 and 6; C) Sites 4 and 5. Amino acids included in each binding site are listed in Table 1.

experiments.

3. Results

3.1. Identification of DMPO binding sites and energy interaction within the TLR2-TIR domain

Because several TLRs share a region called BB-loop which is responsible for signal transduction [16] we hypothesize that the effects of DMPO could be explained by direct binding to BB-loop region within TLRs. Because TLR2 TIR domain is the only one crystallized, we performed a preliminary blind docking analysis using the Lamarckian genetic algorithm [18] on this domain. The solutions were sorted in terms of ΔGbind, and the lowest docking energy conformations of each cluster were considered to be the most stable orientations. Fortunately, the surface of TIR is not very extensive (only 149 residues long) and therefore only six different putative sites where DMPO can bind were found (Fig. 2). Fig. 2A shows the topology of site 2 and specific residues located in there, whereas Fig. 2B, shows the topology of sites 1, 3 and 6; and Fig. 2C shows the topology of sites 4 and 5.

In a second stage, six molecular dynamic simulations were performed, starting from the coordinates of each representative of the best ranked TIR-DMPO complexes (C1–C6), which were obtained from the blind docking experiment. The complexes were subjected to 20.0 ns MD simulation and results are shown in Table 1.

Furthermore, we calculated the relative binding free energies (ΔΔGbind) of the 6 complexes listed above in order to identify the structural thermodynamic characteristics of the binding site into the TIR domain. Results are shown in Table 2. It should be noted that the inadequacies of the models, the implicit limitations of the method, and the simplifications in its applications should be canceled when the relative free energies (ΔΔGbind) rather than absolute (ΔGbind) energies are calculated [33].

Considering the results displayed in Table 2, complex 2 emerges as the best ranked from the six analyzed complexes. Noteworthy, site 2 is located in the BB-loop adjacent to the conserved residues P681 and G682. This result was highly encouraging because the identified binding site where DMPO fits the TIR domain has previously been

Table 1
Summary of results obtained from blind docking analysis. Free energy of the TIR-DMPO complexes are shown here.

Potential binding pocket (Site)	Member in cluster	Lowest energy	Residues located at < 5 Å from the best-docked conformation
1	131	−4.54	I693, H697, K698, T699, F3722, N729, D730, A731, I733
2	41	−4.09	Y641, D678, I680, K683, D687, N688, D691, S692, K695
3	104	−4.01	A732, I733, L734, I735, T760, Y761, L762
4	17	−3.84	L736, L737, E738, P739, L762, E763, W764, P765
5	3	−3.75	Y761, L762, E763, P765, Q770, G763, F774, N777
6	4	−3.38	R675, F679, I680, K683, W684, I685, I686, D687, N688

found to be important in downstream signaling [17]. To investigate which residues within the binding site, identified as located in complex 2, are responsible for the binding affinities for DMPO, an energy decomposition analysis was performed. Fig. 3 shows the results of plotting the ΔGtot contribution *versus* each TIR residue. The binding between TIR and DMPO located at binding site 2 is driven by selected "hot spots" that play a major role in TIR-DMPO recognition. The most important residues are D678, F679, I680, K883, and K695 which were found to be involved in several non-covalent interactions with DMPO. It should be noted that the molecular interaction with K683 is the strongest one, and therefore it appears that such interaction might be one of the anchoring points which stabilize the complex. In addition, other interactions somewhat weaker with Y641, S682, D687, and N688 complete the interactions to stabilize the complex.

3.2. Evaluation of the molecular interactions (MI) of the TIR-DMPO complex using QTAIM calculations

The topological analysis of the electron density constitutes a powerful tool to investigate the electronic properties of a molecular system and allows a deep examination of the molecular interactions. We have demonstrated that utilizing QTAIM calculations, it is possible to determine in an unequivocal way, the different interactions (strong and weak ones) between two atoms throughout the existence of bond critical points (BCPs) and their respective bond paths. Thus, the intermolecular interactions of the complex TIR-DMPO were evaluated using the QTAIM technique. Results are summarized in Fig. 4. These are the sum of the charge density values at the intermolecular BCPs between DMPO and specific amino acid residues at the BB-loop region within of TIR domain are shown. Fig. 4 also shows four anchor points: Y641, K683, N688, and N691. It is important to note that K683 presents a strong hydrogen bond with DMPO, whereas the hydrogen bonds formed with the other amino acid residues are moderate. Moreover, the residues F679, I680, N688 establish several hydrophobic interactions with DMPO that although they are individually weak, as a whole they significantly contribute to the overall binding energy, and probably to the function of such interaction.

To better appreciate the different MIs obtained in this complex, the interactions were also displayed using two alternative illustrations. Fig. 5a showing the main hydrophobic interactions observed for the DMPO-TIR complex and Fig. 5b showing the most relevant polar interactions obtained for the complex.

3.3. Inhibition of toll-like receptor 2 signaling by DMPO

Blind docking, molecular dynamics and QTAIM calculation descript the most likely interaction between DMPO and the BB-loop region at the TLR2-TIR domain responsible for downstream signal transduction. In order to test whether our *in silico* simulations had a functional consequence we assessed the effect of DMPO on TLR2 signaling using transient transfection of NF-κB reporter plasmid into HEK293 cells transfected with human TLR2.6 and then we stimulated them with zymosan in the presence or in the absence of DMPO. The results showed an inhibitory effect of DMPO on zymosan-triggered TLR2 signaling when added to culture medium (Fig. 6).

3.4. Effect of DMPO on TLR2-MyD88 coupling

It has been reported that inhibition of TLR2 signaling can be achieved using small peptides targeting the BB-loop region of TIR causing disruption of TLR2-MyD88 interaction [17]. Based on this piece of evidence and our *in silico* and *in vitro* data, we tested the effect of DMPO on TLR2-MyD88 protein-protein interaction using the co-immunoprecipitation technique in macrophage-like cells derived from THP-1 cell line. It is important to highlight the fact that THP-1 cells used in this experiment have to be properly differentiated into macrophage-like cells using phorbol 12-myristate 13-acetate (PMA), before TLR2 stimulation [34]. This previous step may affect the basal level of TLR2-MyD88 coupling, thus affecting our results.

Results shown in Fig. 7 indicate that the presence of the spin trap does not block zymosan-induced protein-protein interaction between TLR2 and its adaptor protein MyD88.

4. Discussion

Herein we have determined and measured, for the first time, the interaction between DMPO and four-specific residues within the BB-loop region of TLR2 TIR domain, and its functional consequences in

Table 2
Free energy results of the best ranked TIR-DMPO complexes (C).

Component	C1		C2		C3		C4		C5		C6	
	Mean[a]	Std[b]	Mean	Std	Mean	Std	Mean	Std	Mean	Std	Mean	Std
ΔE_{vdW}	−17.46	1.30	−19.40	1.03	−16.19	1.07	−17.30	1.17	−14.20	0.96	−14.56	0.82
ΔE_{ele}	−5.63	0.59	−5.83	0.57	−1.68	0.45	0.41	0.42	−1.32	0.32	−0.38	0.38
ΔG_{PB}	9.89	0.53	11.74	0.60	4.45	0.35	5.43	0.49	4.25	0.27	5.70	0.44
ΔG_{SASA}	−1.94	0.02	−1.85	0.02	−1.57	0.03	−1.72	0.02	−1.49	0.02	−1.63	0.02
ΔE_{gas}	−23.09	1.21	−25.23	1.05	−17.87	1.07	−16.89	1.18	−15.51	1.05	−14.94	0.89
ΔG_{solve}	7.96	0.53	9.89	0.60	2.88	0.34	3.70	0.48	2.76	0.26	4.07	0.43
ΔG_{Bind}	−15.13	1.26	−15.34	1.03	−14.99	1.04	−13.19	1.27	−12.75	0.96	−10.87	0.90
$\Delta\Delta G_{Bind}$	0.21		0.00		0.35		2.16		2.59		4.47	

[a] Average value.
[b] Standard deviation.

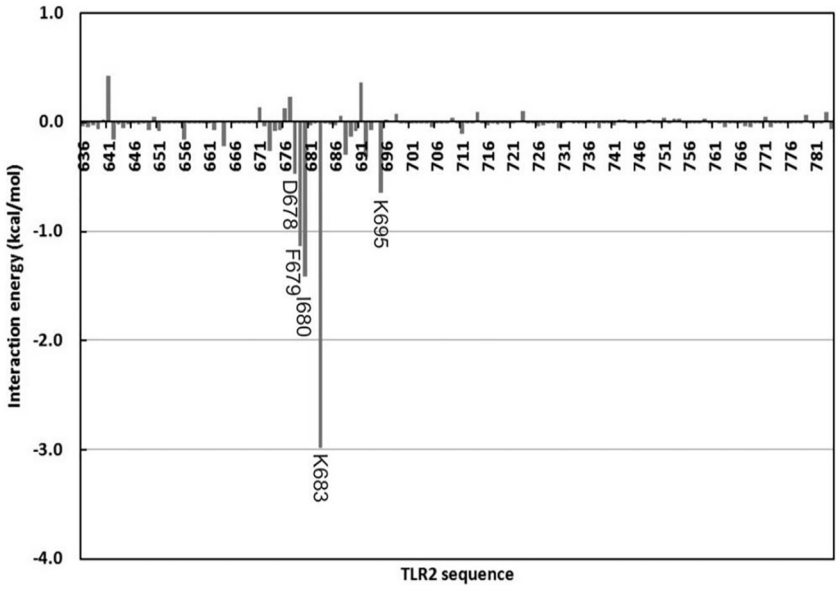

Fig. 3. Histogram of the interaction energies partitioned with respect to the TIR-DMPO complex 2. The x-axis denotes the residue number of TIR domain, and the y-axis denotes the interaction energy between DMPO and specific amino acid residues within the potential binding pocket (site) 2 at the TIR domain. These amino acid residues composing site 2 are located at the BB-loop region within the TLR2-TIR domain.

signaling. To our knowledge, this is the first evidence showing the mechanism of DMPO dampening TLR2 signaling that may be extended to other TLRs, such as TLR4.

Mistry et al. have provided convincing data showing that targeting the BB loop pocket is an effective approach for the identification of TLR2 signaling inhibitors [35]. In our study, the combination of blind docking and subsequent MD simulations indicated that site 2 is the most likely to which DMPO would be bound in TLR2-TIR domain. This site where DMPO fits into the TIR domain has been previously found to be important in downstream signaling [17]. Particularly, residue P681 has a critical role in TLR2 triggered signaling as shown by site-directed mutagenesis technique [17,35]. Moreover, a naturally occurring allele of mouse TLR4 has been reported to be unresponsive to LPS due to a point mutation on residue P712, a structural analog of human TLR2 P681 residue [16,17].

The evaluation of the molecular interactions of the TIR-DMPO complex by using QTAIM calculations indicates that the complex shows four main anchor points: Y641, K683, N688, and N691. Whereas K683 presents a strong hydrogen bond, the other hydrogen bonds are moderate. On the other hand, the residues F679, I680, N688 presents several hydrophobic interactions with DMPO that although they are individually weak, as a whole (making an additive effect) they contribute significantly to the stability of the complex. From our results, a complete structural description for this DMPO-binding site, including the different interaction stabilizing the TIR-DMPO complex, has been obtained. The full coordinates of this complex are available as supplementary material (See Supplementary materials).

Protein-protein interactions between the TLR2-TIR-BB-Loop domain with the BB-loop within MyD88 are important to ensure functional downstream signaling. Thus, according to our *in silico* data, we tested whether by non-covalently binding to those specific residues at the BB-loop domain DMPO may reduce the effective downstream signaling. To test this possibility we measured the functional effects of DMPO on zymosan-triggered TLR2 signaling and found that DMPO inhibits downstream signaling. It is important to highlight that the HEK293 cells do not express TLRs [36], hence our findings on TLR2 signaling are only linked to this specific receptor. These results support ours *in silico* simulations where DMPO was found to directly bind to a key region responsible for signal transduction, *i.e.,* the BB-loop within the TLR2-TIR domain. DMPO interferes the signaling triggered by zymosan-induced protein-protein interaction between TLR2-TIR-BB-loop with its adaptor protein MyD88.

Because DMPO inhibits the function of the TLR2-TIR-BB-loop/MyD88 protein-protein interaction, it may be because DMPO binds to a

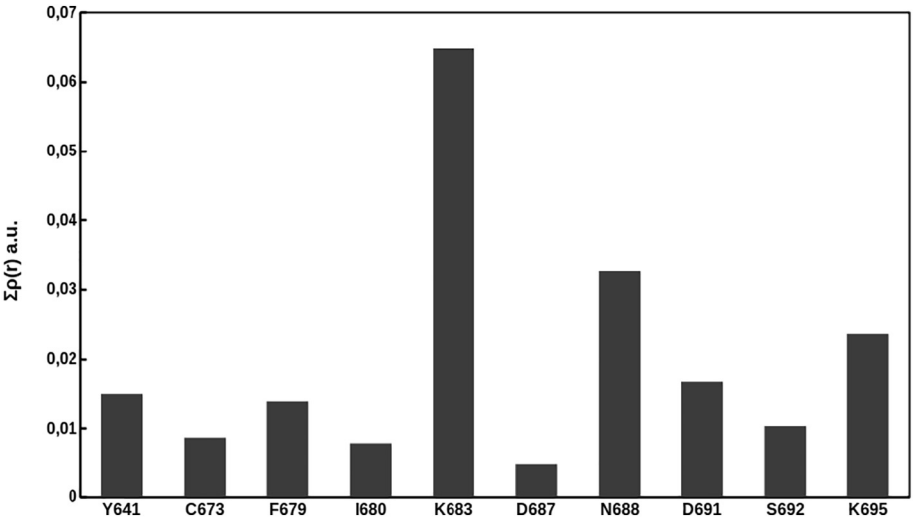

Fig. 4. Overall interaction energy between specific amino acid residues at the TLR2-TIR-BB-loop region and DMPO. Sum of the values of charge density ($\Sigma\rho(r)$) resulting from hydrogen bonds and hydrophobic interactions established between specific amino acid residues at the BB-Loop region and DMPO. The BB-Loop is located at the potential binding site 2 within the TLR2-TIR domain. Only the intermolecular interactions are added in the sum. a.u., arbitrary units.

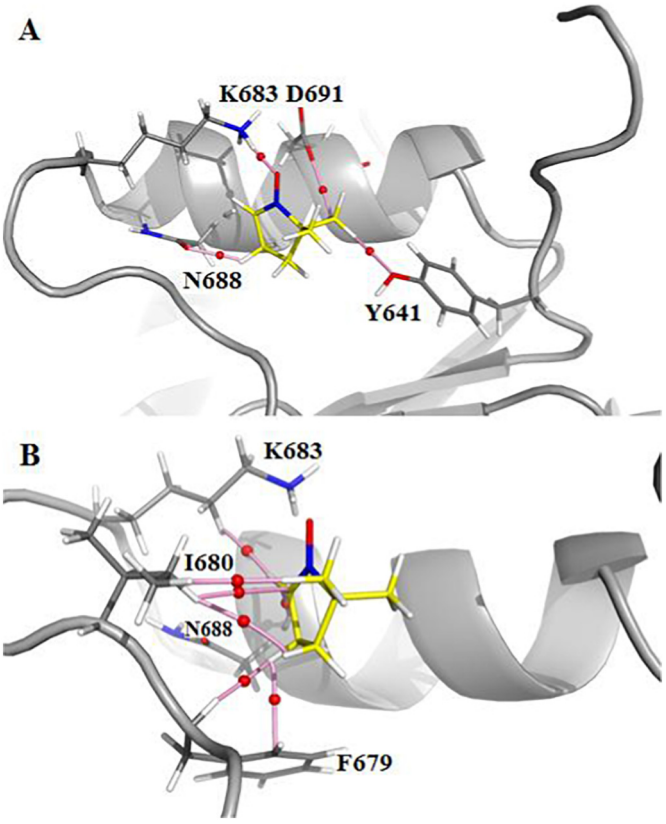

Fig. 5. Non-covalent interactions between DMPO and specific residues within the TLR2-TIR-BB-loop region. DMPO structure is shown as yellow sticks. A) hydrogen bond interactions and B) hydrophobic interactions. The elements of the electron density topology are shown. The bond paths connecting each nucleus are shown as pink sticks and the bond critical points are shown as red spheres.

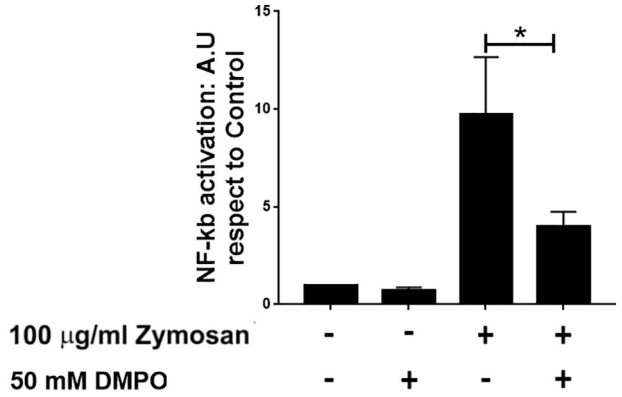

Fig. 6. Functional determination of the effect of DMPO on zymosan-triggered TLR2-mediated NF-κB activation. HEK293 hTLR2.6-expressing cells were transfected with the NF-κB-reporter construct to test TLR2 signaling specifically. Then cells were treated with TLR2 stimulus (100 μg/mL zymosan) in the presence or in the absence of 50 mM DMPO. TLR-2-mediated NF-κB activation was measured as SEAP activity as described in the Materials and Methods section. Culture medium was used as the control. All experiments were independently repeated at least 3 times by triplicate in each experiment. Results are shown as mean values ± SEM. * P value < 0.01. A.U., arbitrary units.

critical site needed for this interaction. In other words, by binding to one or more specific amino acid residues within the TLR2-TIR-BB-loop region DMPO may block the binding of TLR2-TIR with MyD88. Thus we measured the effect of DMPO on the binding of TLR2 with MyD88 upon zymosan activation in THP-1-derived macrophages. Our co-

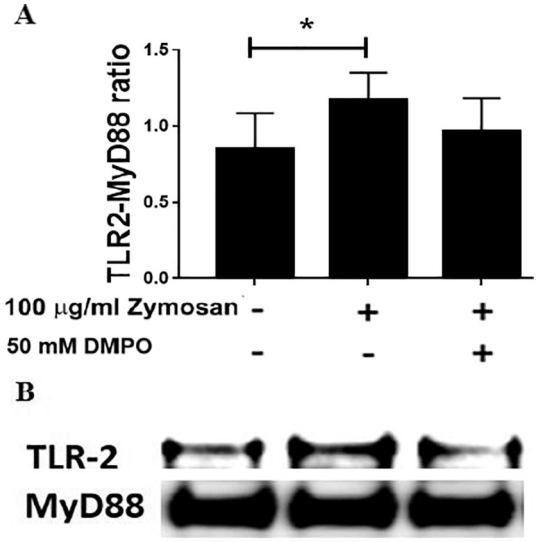

Fig. 7. Effect of DMPO on TLR2-MyD88 protein-protein interaction after zymosan triggered TLR2 signaling in macrophages. Human macrophage-like cells were differentiated from THP-1 cells by treatment with PMA. Then TLR2 signaling was triggered with 100 μg/mL zymosan in the presence or in the absence of 50 mM DMPO for 15 min. Co-immunoprecipitation was performed using anti-TLR2 antibody and anti-MyD88 antibody. A) The optical density of immunoprecipitated proteins. Pulled-down proteins were analyzed as described in the Materials and Methods section. Results are shown as mean values ± SEM of the TLR2-My88 ratios. * P value < 0.05. B) Picture of the most representative western-blot image.

immunoprecipitation data suggest that DMPO does not inhibit TLR2-MyD88 protein-protein interaction. However, this observation does not necessarily mean that DMPO binding to the BB-loop inhibits, in term of downstream signaling, the functionality of the TLR2-MyD88 protein-protein interaction. The spin trap could be disrupting the proper interaction of TLR2 with the adaptor protein without completely inhibiting the protein-protein interaction. These findings are consistent with our previously published data and propose an explanation for the observed phenomenon of multiple TLRs inhibition by DMPO, as we have previously reported [11].

Our data and the fact that TIR-BB-loop region is conserved throughout different TLRs and species empowers further studies of the effects of DMPO on other TLRs and encourages the use of nitrone spin traps (or their derivates) as mechanism-based anti-inflammatory drugs.

Transparency Document

The Transparency document associated with this article can be found, in online version.

Conflict of interest

Authors declare that no conflict of interest exists.

Acknowledgments

Authors are thankful to Dr. Paula Di Sciullo for her excellent technical assistance. This research was supported by the following research awards: FONCYT-Argentina (PICT-2014-3369, to DCR), CONICET-Argentina (PIP-916, to DCR and SEGM), and National University of San Luis-Argentina (PROICO 02-3418 to DCR and PROICO 10-0218, to SEGM). DCR and SEGM want to dedicate this article to their former mentors Dr Ronald P. Mason, Dr Robert A. Floyd and Dr Maria S. Gimenez for seminal scientific contributions to the data published here.

Appendix A. Supplementary data

Supplementary data to this article can be found online at https://doi.org/10.1016/j.bbadis.2019.01.005.

References

[1] E.G. Janzen, Spin trapping, Methods Enzymol. 105 (1984) 188–198.
[2] E.G. Janzen, J.L. Poyer, C.F. Schaefer, P.E. Downs, C.M. DuBose, Biological spin trapping. II. Toxicity of nitrone spin traps: dose-ranging in the rat, J. Biochem. Biophys. Methods 30 (1995) 239–247.
[3] E.G. Janzen, M.S. West, Y. Kotake, C.M. DuBose, Biological spin trapping methodology. III. Octanol-water partition coefficients of spin-trapping compounds, J. Biochem. Biophys. Methods 32 (1996) 183–190.
[4] R.A. Floyd, R.D. Kopke, C.H. Choi, S.B. Foster, S. Doblas, R.A. Towner, Nitrones as therapeutics, Free Radic. Biol. Med. 45 (2008) 1361–1374.
[5] Z. Zhai, S.E. Gomez-Mejiba, H. Zhu, F. Lupu, D.C. Ramirez, The spin trap 5,5-dimethyl-1-pyrroline *N*-oxide inhibits lipopolysaccharide-induced inflammatory response in RAW 264.7 cells, Life Sci. 90 (2012) 432–439.
[6] T. Tabatabaie, A.M. Vasquez, D.R. Moore, R.A. Floyd, Y. Kotake, Direct administration of interleukin-1 and interferon-gamma to rat pancreas leads to the in vivo production of nitric oxide and expression of inducible nitric oxide synthase and inducible cyclooxygenase, Pancreas 23 (2001) 316–322.
[7] E. Finkelstein, G.M. Rosen, E.J. Rauckman, J. Paxton, Spin trapping of superoxide, Mol. Pharmacol. 16 (1979) 676–685.
[8] X. Du, M.B. West, Q. Cai, W. Cheng, D.L. Ewert, W. Li, R.A. Floyd, R.D. Kopke, Antioxidants reduce neurodegeneration and accumulation of pathologic Tau proteins in the auditory system after blast exposure, Free Radic. Biol. Med. 108 (2017) 627–643.
[9] S.E. Gomez-Mejiba, Z. Zhai, H. Akram, L.J. Deterding, K. Hensley, N. Smith, R.A. Towner, K.B. Tomer, R.P. Mason, D.C. Ramirez, Immuno-spin trapping of protein and DNA radicals: “tagging” free radicals to locate and understand the redox process, Free Radic. Biol. Med. 46 (2009) 853–865.
[10] Z. Zhai, S.E. Gomez-Mejiba, M.S. Gimenez, L.J. Deterding, K.B. Tomer, R.P. Mason, M.T. Ashby, D.C. Ramirez, Free radical-operated proteotoxic stress in macrophages primed with lipopolysaccharide, Free Radic. Biol. Med. 53 (2012) 172–181.
[11] M.D. Munoz, M.C. Della Vedova, P.R. Bushel, D. Ganini da Silva, R.P. Mason, Z. Zhai, S.E. Gomez Mejiba, D.C. Ramirez, The nitrone spin trap 5,5-dimethyl-1-pyrroline N-oxide dampens lipopolysaccharide-induced transcriptomic changes in macrophages, Inflamm. Res. 67 (2018) 515–530.
[12] J.K. Li, J.J. Balic, L. Yu, B. Jenkins, TLR agonists as adjuvants for Cancer vaccines, Adv. Exp. Med. Biol. 1024 (2017) 195–212.
[13] D.W. Good, T. George, B.A. Watts 3rd, Toll-like receptor 2 is required for LPS-induced toll-like receptor 4 signaling and inhibition of ion transport in renal thick ascending limb, J. Biol. Chem. 287 (2012) 20208–20220.
[14] O. Takeuchi, K. Hoshino, T. Kawai, H. Sanjo, H. Takada, T. Ogawa, K. Takeda, S. Akira, Differential roles of TLR2 and TLR4 in recognition of gram-negative and gram-positive bacterial cell wall components, Immunity 11 (1999) 443–451.
[15] H. Ohnishi, H. Tochio, Z. Kato, K.E. Orii, A. Li, T. Kimura, H. Hiroaki, N. Kondo, M. Shirakawa, Structural basis for the multiple interactions of the MyD88 TIR domain in TLR4 signaling, Proc. Natl. Acad. Sci. U. S. A. 106 (2009) 10260–10265.
[16] T. Ve, P.R. Vajjhala, A. Hedger, T. Croll, F. DiMaio, S. Horsefield, X. Yu, P. Lavrencic, Z. Hassan, G.P. Morgan, A. Mansell, M. Mobli, A. O'Carroll, B. Chauvin, Y. Gambin, E. Sierecki, M.J. Landsberg, K.J. Stacey, E.H. Egelman, B. Kobe, Structural basis of TIR-domain-assembly formation in MAL- and MyD88-dependent TLR4 signaling, Nat. Struct. Mol. Biol. 24 (2017) 743–751.
[17] S. Basith, B. Manavalan, R.G. Govindaraj, S. Choi, In silico approach to inhibition of signaling pathways of toll-like receptors 2 and 4 by ST2L, PLoS One 6 (2011) e23989.
[18] J. Fuhrmann, A. Rurainski, H.P. Lenhof, D. Neumann, A new Lamarckian genetic algorithm for flexible ligand-receptor docking, J. Comput. Chem. 31 (2010) 1911–1918.
[19] K. Lindorff-Larsen, S. Piana, K. Palmo, P. Maragakis, J.L. Klepeis, R.O. Dror, D.E. Shaw, Improved side-chain torsion potentials for the Amber ff99SB protein force field, Proteins 78 (2010) 1950–1958.
[20] J. Wang, R.M. Wolf, J.W. Caldwell, P.A. Kollman, D.A. Case, Development and testing of a general amber force field, J. Comput. Chem. 25 (2004) 1157–1174.
[21] L. Larini, R. Mannella, D. Leporini, Langevin stabilization of molecular-dynamics simulations of polymers by means of quasisymplectic algorithms, J. Chem. Phys. 126 (2007) 104101.
[22] H. Wang, X. Gao, J. Fang, Multiple staggered mesh Ewald: boosting the accuracy of the smooth particle mesh Ewald method, J. Chem. Theory Comput. 12 (2016) 5596–5608.
[23] S. Genheden, U. Ryde, The MM/PBSA and MM/GBSA methods to estimate ligand-binding affinities, Expert Opin. Drug Discovery 10 (2015) 449–461.
[24] E. Brunk, U. Rothlisberger, Mixed quantum mechanical/molecular mechanical molecular dynamics simulations of biological systems in ground and electronically excited states, Chem. Rev. 115 (2015) 6217–6263.
[25] Y. Zhao, The M06 suite of density functionals for main group thermochemistry, thermochemical kinetics, noncovalent interactions, excited states, and transition elements: two new functionals and systematic testing of four M06-class functionals and 12 other functionals, Theor. Chem. Accounts 120 (2007) 215–241.
[26] K.M. Marz, C.I. Bayly, D.M. Ferguson, W.D. Cornell, T. Fox, J.W. Caldwell, P.A. Kollman, P. Cieplak, I.R. Gould, D.C. Spellmeyer, A second generation force field for the simulation of proteins, nucleic acids, and organic molecules, J. Am. Chem. Soc. 117 (1995) 5179–5197.
[27] R.F.W. Bader, Atoms in molecules, Acc. Chem. Res. 18 (1985) 9–15.
[28] T. Lu, F. Chen, Multiwfn: a multifunctional wavefunction analyzer, J. Comput. Chem. 33 (2012) 580–592.
[29] E.E. Barrera Guisasola, L.J. Gutiérrez, R.E. Salcedo, F.M. Garibotto, S.A. Andujar, R.D. Enriz, A.M. Rodríguez, Conformational transition of Aβ42 inhibited by a mimetic peptide. A molecular modeling study using QM/MM calculations and QTAIM analysis, Comput. Theor. Chem. 1080 (2016) 56–65.
[30] L.J. Gutierrez, E.E. Becerra Guisasola, N. Peruchena, R.D. Enriz, A QM/MM study of the molecular recognition site of bapineuzumab toward the amyloid-β peptide isoforms, Mol. Simul. 42 (2015) 196–207.
[31] E.G. Vega-Hissi, R. Tosso, R.D. Enriz, L.J. Gutierrez, Molecular insight into the interaction mechanisms of amino-2H-imidazole derivatives with BACE1 protease: a QM/MM and QTAIM study, Int. J. Quantum Chem. 115 (2014) 389–397.
[32] C.A. Schneider, W.S. Rasband, K.W. Eliceiri, NIH image to ImageJ: 25 years of image analysis, Nat. Methods 9 (2012) 671–675.
[33] B.J. Williams-Noonan, E. Yuriev, D.K. Chalmers, Free energy methods in drug design: prospects of "alchemical perturbation" in medicinal chemistry, J. Med. Chem. 61 (2018) 638–649.
[34] M. Zou, L. Xi, J. Rao, Y. Jing, F. Liao, X. Yang, Optimization and evaluation of an inflammatory cell model in LPS-stimulated PMA-differentiated THP-1 cells, Xi bao yu fen zi mian yi xue za zhi 33 (2017) 1456–1461.
[35] P. Mistry, M.H. Laird, R.S. Schwarz, S. Greene, T. Dyson, G.A. Snyder, T.S. Xiao, J. Chauhan, S. Fletcher, V.Y. Toshchakov, A.D. MacKerell Jr., S.N. Vogel, Inhibition of TLR2 signaling by small molecule inhibitors targeting a pocket within the TLR2 TIR domain, Proc. Natl. Acad. Sci. U. S. A. 112 (2015) 5455–5460.
[36] P. Thomas, T.G. Smart, HEK293 cell line: a vehicle for the expression of recombinant proteins, J. Pharmacol. Toxicol. Methods 51 (2005) 187–200.